ECS Transactions, 33 (6) 813-821 (2010)
10.1149/1.3487611 ©The Electrochemical Society

Elastically Strain-Sharing Si(110) Nanomembranes

Deborah M. Paskiewicz, Shelley A. Scott, Donald E. Savage, and Max G. Lagally

Department of Materials Science and Engineering, University of Wisconsin-Madison, Madison, Wisconsin 53706, USA

Defect-free, smooth, tensilely strained Si(110) has been fabricated via elastic strain relaxation of trilayer $Si/Si_{(1-x)}Ge_x/Si(110)$ nanomembrane heterostructures grown on silicon-on-insulator (SOI), in which the middle layer is compressively strained. We release these trilayer structures via selective etching to allow elastic strain sharing between the $Si/Si_{(1-x)}Ge_x/Si(110)$ layers, thus creating tensilely strained Si(110). We use low-temperature molecular beam epitaxy (MBE) to grow the SiGe and top Si layers to create smooth films and incorporate more strain in the Si(110) layers; the low growth temperatures suppress relaxation, allowing for thicker SiGe(110) films. The strain in the Si(110) layers can be controlled with elastic strain engineering up to ~0.7%.

Introduction

With scaling techniques reaching practical limits for the enhancement of current complementary metal-oxide-semiconductor (CMOS) technologies, materials modifications in Si, such as incorporation of strain and changes in crystal orientation, have become necessary to increase device performance. Strain engineering of Si(001), for example, is well established and significant improvements in charge carrier mobility have been realized with both process-induced (local) and substrate-induced (global) straining techniques (1, 2); with a combination of the two techniques producing maximum enhancements in mobility (3). However even with the advantages gained from strain, the hole mobility is still significantly lower than the electron mobility on (001)-oriented Si. This produces large current drive imbalances between n- and p-type devices for CMOS. Strained Si(110) has emerged as an attractive option for p-MOS and CMOS devices, not only because the (110) orientation of Si has the highest hole mobility (4, 5), but both electron and hole charge carrier mobilities are enhanced with the addition of strain (6, 7). Local straining techniques have been used to improve charge carrier mobility in Si(110) (8), however the advantages obtained from multiple stressors (global + local) (9) cannot be fully realized unless there is a good way of fabricating global strain in (110)-oriented Si without large densities of extended defects. Global straining techniques typically involve the growth of strained Si on a relaxed SiGe layer (10, 11). Pseudomorphically growing Si on the larger-lattice-constant SiGe layer will result in a biaxial tensile strain in the Si. Creating large areas of high-quality, biaxially strained Si(110) from conventional relaxed $Si_{(1-x)}Ge_x(110)$ has been difficult because of the crystal anisotropy of the (110) orientation (12): high dislocation densities (13), rough growth fronts (14, 15), anisotropic strain relaxation of SiGe(110) (12, 16, 17), and strain inhomogeneities (18), can lead to significant device degradation. In this paper we report on the use of our elastic strain sharing nanomembrane (NM) technique (19) to fabricate strained, crystalline Si(110) sheets. This method involves elastic strain transfer between layers of a

pseudomorphically grown Si/$Si_{(1-x)}Ge_x$/Si(110) trilayer stack. Low-temperature molecular beam epitaxy (MBE) growth of the tri-layer Si(110) NMs results in smooth, coherent films, which are released from the handling substrate and allowed to relax elastically. We show that the strain in the Si(110) layers can be controllably tuned up to ~0.7%. Furthermore, these NMs can be transferred and bonded to a variety of other substrates while maintaining uniform biaxial strain.

Experimental

Elastically strain-shared Si(110) NMs are fabricated in the manner we have developed for Si(001) (19), by growing heterostructures of Si/$Si_{(1-x)}Ge_x$/Si(110) on SOI (110) and releasing them by etching the buried oxide (BOX). This process is shown schematically in Figure 1. The SiGe and top Si layers are pseudomorphically grown with solid-source MBE on the Si(110) template layer (Fig. 1a). After growth, etchant access holes are patterned into the trilayer NM (Fig. 1b), followed by release from the handling substrate by etching away the buried oxide layer of the SOI(110) (Fig. 1c). During the release process this trilayer NM is free and can thus share strain elastically: the compressively strained SiGe middle layer partially relaxes (expands), transferring tensile strain to the sandwiching Si layers. The Si(110) trilayer NM can either settle onto the handling substrate or can be easily transferred to a variety of other substrates (Fig. 1d).

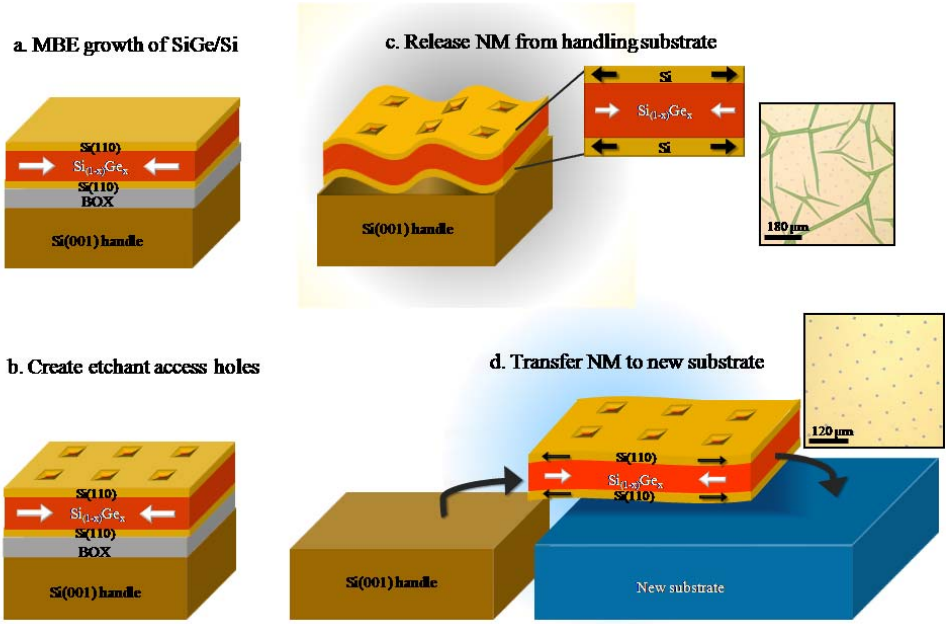

Figure 1. Si/$Si_{(1-x)}Ge_x$/ Si(110) NM fabrication process. (a) MBE growth of SiGe and Si layers on the template layer of SOI(110). (b) Fabrication of etchant access holes with photolithography and reactive ion etching. (c) Removal of BOX layer in 49% HF to create a free-standing trilayer NM. During release from the handling substrate the trilayer is allowed to strain share: some of the compressive strain in the SiGe layer transfers as tensile strain to the Si(110) layers. The trilayer NM temporarily falls back onto the handling substrate. The optical micrograph shows wrinkles because the NM expands during strain sharing. (d) The NM can then be transferred to water where it floats on the surface, allowing easy transfer to new substrates, where it lies flat and exhibits proper elastic strain sharing (optical micrograph after transfer of NM shown in inset).

We used low-temperature MBE to grow smooth, thick, pseudomorphic films of high Ge composition (110)-oriented alloy. A low growth temperature of 450°C resulted in pseudomorphic SiGe films with good crystalline quality. The low-temperature bound was set by the ability to maintain an approximately constant temperature with resistive heating. We determined the crystalline quality and measured the out-of-plane lattice constants of all layers with high-resolution x-ray diffraction (XRD) triple-axis θ/2θ line scans around the (220) reflection before and after release of the trilayer Si(110) NMs. Simulations of the as-grown (220) θ/2θ line scans allowed us to extract exact thicknesses of each layer, and the Ge composition of the alloy layer. Intermittent-contact mode atomic force microscopy (AFM) was used to monitor the surface morphology to check for signs of plastic relaxation in the SiGe layer during growth.

Results and Discussion

Strain Engineering

We have shown that we can control the strain transferred to the Si layers after release of a trilayer NM by varying the thicknesses of each of the layers and the Ge composition of the alloy layer (19, 20). As a review, the strain in the Si layers after strain sharing will be (21):

$$\varepsilon_{Si} = -\frac{1}{1+\frac{t_{Si}}{t_{SiGe}}\frac{M_{Si}}{M_{SiGe}}}\varepsilon_m \qquad [1]$$

where ε_m is the mismatch strain, t is the total layer thickness (for Si it is the sum of both layers), and M is the biaxial modulus of the respective layers (M_{SiGe} is taken as a linear combination of M_{Si} and M_{Ge} based on Vegard's Law). Equation 1 is derived from a force balance model in which the trilayer NM remains flat during elastic strain sharing (the top and bottom Si layers are of equal thickness to ensure the trilayer does not curl to accommodate the mismatch strain (22)). This model also assumes the strain transfer is biaxially isotropic: a proper assumption for strain sharing between similar crystalline materials such as Si and SiGe (20).

As mobility enhancement is typically proportional to the magnitude of strain, a high amount of strain is desired in the Si(110) layers after elastic strain sharing. From Eq. 1 we can say that maximum strain transfer to the Si layers will occur for high mismatch strains (ε_m) and low thickness ratios (t_{Si}/t_{SiGe}). In other words, we can optimize the amount of strain in the Si layers by increasing the Ge composition of the alloy layer, increasing the thickness of the alloy layer, and decreasing the total thickness of the Si layers. However, as we increase the thickness of the alloy layer, while increasing the Ge composition, we will start to relax the SiGe layer plastically: we will reach the critical thickness for dislocation formation (23). We do not want plastic relaxation, because as the alloy layer plastically relaxes, the mismatch strain between the Si and SiGe layers is reduced, thus decreasing the amount of strain that can potentially be transferred to the Si layers. In theory one could imagine transferring large amounts of strain from thick, high-Ge concentration, partially relaxed alloy layers with high mismatch strains, but as the alloy layer starts to relax strain inhomogenities occur and will transfer to the Si layers upon strain sharing. The strain inhomogenities produced in partially relaxed films (on ~1-100nm length scales) have been proven to act as significant scattering mechanisms for charge carriers (24). Therefore to obtain uniform, maximum strain transfer for a given Ge

composition alloy layer, the SiGe layers must be fully compressively strained to the Si lattice constant. This means that the alloy layers must be grown below the kinetic critical thickness limit for dislocation formation (25). The kinetic critical thickness is dependent on growth conditions and growth temperature. Controlling the kinetic critical thickness (and alternatively, the relaxation) of SiGe(110) films is more difficult than the (001) counterpart because there is a larger driving force for dislocation formation on the (110) surface (26): because of partial dislocation formation the thermodynamic critical thickness is lower for SiGe(110) films than SiGe(001) films. It is therefore desirable to use low-temperature growth of the (110) alloys to suppress relaxation (25), to enable growth of thicker, fully strained SiGe(110) films. Epitaxial growth of SiGe(110) with chemical vapor deposition (CVD) is reaction limited (controlled by the H desorption rate from the surface) and requires high temperatures (~660°C) to obtain measureable growth rates (27). The high temperature needed for CVD growth encourages surface diffusion, resulting in significant roughening and dislocation nucleation (28). We use MBE in order to control the deposition rate and growth temperature independently, to suppress relaxation in the SiGe(110) layers and transfer larger amounts of strain to the Si(110) layers during elastic strain sharing.

MBE Growth

It has been shown many times that fully strained films of SiGe(001) can be grown beyond the equilibrium critical thickness (23) for dislocation formation by growing at lower temperatures (25). We obtain results for strained SiGe(110) that are consistent with this picture by growing at 450°C with MBE. As shown by Houghton (25), small decreases in growth temperature can result in large increases in kinetic critical thickness. The strain relaxation model proposed by Houghton shows that the kinetic limit for the onset of relaxation in strained epitaxial growth depends on the stress in the film, the growth temperature, and the time at that growth temperature. Thus by limiting the growth temperature and maintaining reasonable growth rates, we were able to obtain thicker, fully strained SiGe(110) films. However, because SiGe(110) relaxes via partial dislocations, the kinetic critical thickness is still much lower than that of SiGe(001) (26), hence we will still obtain lower strains in Si(110) NMs than in the Si(001) NMs.

Figure 2 shows AFM scans of trilayer Si(110) NMs with various alloy layer thicknesses and Ge compositions. The trilayer shown in Fig. 2a was grown at 650°C and the trilayers in Figs. 2b-d were grown at 450°C (all MBE growth). The surface morphology in Fig. 2a is indicative of microtwin formation: ridges along <110> separated by streaks running parallel to <112> in-plane directions (29). The top Si layer does not significantly smooth out any roughness created by relaxation of the alloy because the Si tends to grow preferentially near the twin boundaries (30). As the growth temperature is lowered, the surface becomes smoother and any signs of relaxation due to roughening, dislocation formation, or micro-twin lamellae disappear. We also confirm the improved crystalline quality of the films with symmetric XRD peaks; sharp alloy layer peaks and strong thickness fringes confirm uniform strain and smooth interfaces (examples in Fig. 3). Many of the alloy films grown here were nearly twice as thick as the kinetic critical thickness values reported by Hull et al. (26), who grew SiGe(110) films at 550°C with MBE.

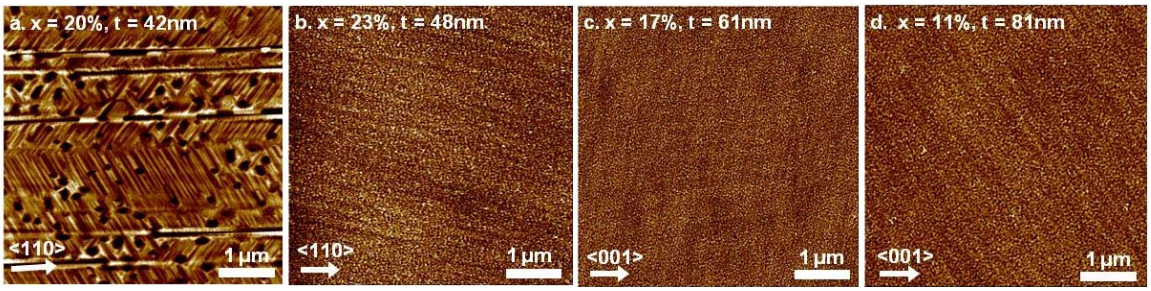

Figure 2. AFM images of the surfaces of trilayer Si(110) NMs grown in MBE at 650°C: (a) Si/~42nm $Si_{.80}Ge_{.20}$/Si(110), and 450°C: (b) 9.5nm Si/49nm $Si_{.77}Ge_{.23}$/9.5nm Si. (c) 15nm Si/61nm $Si_{.23}Ge_{.17}$/14nm Si. (d) 9nm Si/81nm $Si_{.89}Ge_{.11}$/10nm Si. The root-mean-square (rms) roughness for image (a) is 1.8nm, with a z-height scale of 10nm. The rms roughness for images (b), (c), and (d) is ~ 0.4nm, with a z-height scale of 2.5nm. The tensile strain in these three NMs ranges from ~0.65% in (a) to ~0.30% in (c). *x* is the Ge fraction and t is the thickness of the middle layer.

We were also able to lower the RMS roughness significantly with low-temperature growth (0.4nm for low-temperature MBE *vs*. > 1nm for CVD grown structures). The lower growth temperature suppresses lateral diffusion, slowing roughening and allows for the growth of smoother, higher-Ge-concentration alloy layers (28, 31). The RMS roughness for the MBE grown strained-Si(110) NMs (0.65% strain) is comparable to the roughness of CVD grown strained-Si(001) NMs (strain ~0.80%) (19), which exhibit enhanced mobility in MOS thin-film transistors (32). It is important to create smooth strained films, such that the enhancements seen from strain are not negated by surface roughness scattering of charge carriers.

Strain-Sharing in Si(110) NMs

Once optimal-thickness structures are grown with MBE, the strain transferred to the Si layers upon trilayer membrane release is measured with high-resolution XRD. We use out-of-plane triple-axis θ/2θ line scans around the (220) reflection to characterize layer thicknesses, Ge composition, and the out-of-plane strain change. As mentioned above, the structural parameters (layer thicknesses and Ge composition) are extracted from simulations fit to the (220) θ/2θ line scans of the as-grown structures, where all the strain (compressive) is in the SiGe layer. The exact structural parameters allow us to calculate the expected strain transfer to the Si(110) layers upon strain sharing with Eq. 1. We have shown in other publications (15, 20) that we can extract the in-plane strain in the Si(110) layers from measurement of the out-of-plane strain change in the alloy layer. Examples of θ/2θ line scans around the (220) reflection before and after release are shown in Fig. 3 (a θ/2θ scan around the (004) reflection of the Si(001) bulk substrate is used as reference). The most intense peak is from the SiGe layer and indicates a reduction in the out-of-plane lattice constant (increase in Bragg angle). This result is consistent with the notion that the SiGe layer becomes less compressively strained after elastic strain sharing: the reduction in compressive strain in the SiGe layer is transferred as tensile strain to the Si layers. The measurements in Fig. 3 indicate an out-of-plane strain change of 0.23% and 0.27% for thickness ratios of ~0.7 and ~0.5, respectively. The exact trilayer heterostructures are shown in the insets of Figs. 3a and b. The larger change in strain occurs for the lower thickness ratio, which is consistent with the calculation of strain transfer obtained with Eq. 1.

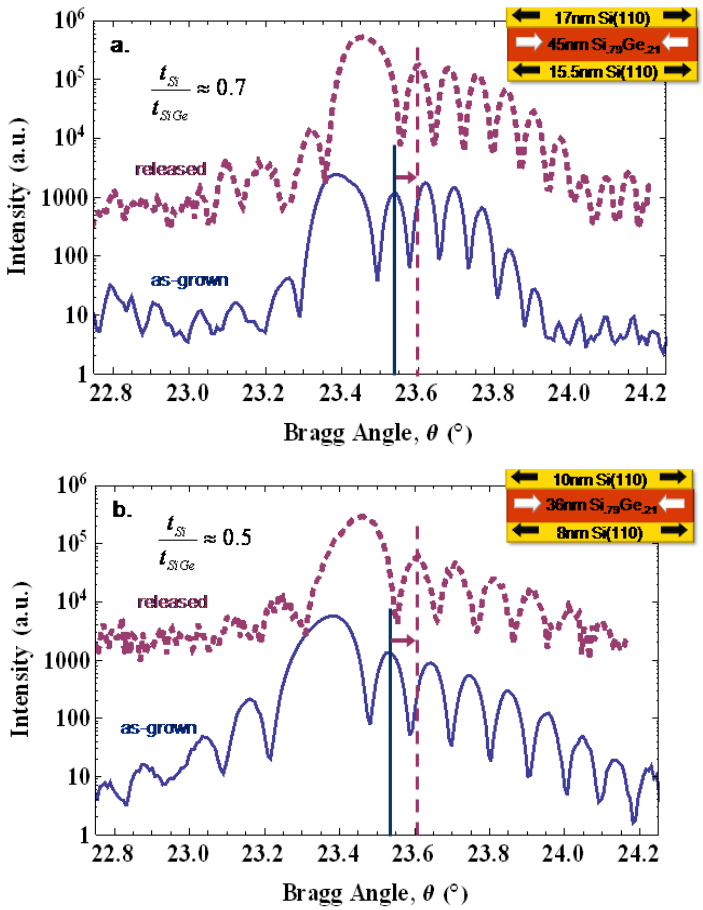

Figure 3. High-resolution θ/2θ XRD line scans around the (220) reflection for two trilayer Si(110) NMs with different thickness ratios [$t_{Si}/t_{SiGe} \approx 0.7$ (a) and ≈ 0.5 (b)] before (solid) and after release (dashed) from the handling substrate. The exact trilayers are shown in the schematicinsets in each figure. The trilayer NMs in both (a) and (b) were transferred to other substrates upon release from the handling substrate. The uniform shift to a higher Bragg angle indicates a decrease in the out-of-plane lattice constant for the entire heterostructure. The out-of-plane strain, (a) $\varepsilon_{\perp} = 0.23 \pm 0.02\%$ and (b) $\varepsilon_{\perp} = 0.27 \pm 0.03\%$, translates to an in-plane strain transfer of (a) $\varepsilon_{||} = 0.46 \pm 0.03\%$ and (b) $\varepsilon_{||} = 0.55 \pm 0.05\%$ to the Si(110) layers.

The relationship between in-plane strain ($\varepsilon_{||}$) and out-of-plane strain ($\varepsilon_{\perp}$) for (110)-oriented cubic materials follows from elastic theory (33):

$$\varepsilon_{||} = -\varepsilon_{\perp} \frac{c_{11} + c_{12} + 2c_{44}}{c_{11} + 3c_{12} - 2c_{44}} \qquad [2]$$

Here c_{ij} are the elastic constants (34) from the elastic stiffness tensor for SiGe; the SiGe elastic constants are obtained by using Vegard's law with the appropriate Ge composition as measured in the as-grown structure. If the strain transfer is truly elastic, the in-plane strain change in the alloy layer upon release, as calculated with Eq. 2, will equal the amount of tensile strain in the Si(110) layers. From the uniformity of the shift of all the

peaks, and the presence of sharp thickness fringes, we can say that the layers remain coherent through the strain sharing process and that the strain transfer is elastic. It should be noted that this condition continues to hold for trilayer NMs that are transferred to other substrates: the transfer process does not introduce any dislocations that would change the strain state of the system.

Table 1 shows the structure of several Si(110) NMs with the corresponding in-plane strain in the Si layers. The expected strain is calculated from Eq. 1 and the measured strain extracted from the shift in (220) XRD line scans and Eq. 2. Thus far, we have been able to achieve a maximum strain of ~0.65% in Si(110) with elastic strain sharing by reducing the thickness ratio between Si and SiGe; a result of using thin Si layers and increasing the SiGe thickness with low-temperature MBE growth. The strain transferred to the Si(110) layers is highly controllable and uniform. By using *elastic* strain sharing we can induce strain in Si(110) without the high densities of defects inherent in growing strained Si(110) on plastically relaxed SiGe(110) substrates (13), which may limit the mobility enhancement achieved with strain (24). Previous mobility measurements for pMOSFETs created on ~0.6% biaxially, tensilely strained Si(110) resulted in a 20-30% increase in hole and electron mobilities over the unstrained-Si(110) values (6). These measurements come from strained Si(110) fabricated on relaxed-SiGe substrates (created via the Ge condensation technique (17)), which can exhibit poor material quality. One can expect that mobility enhancement due to strain may be limited by interface roughness, inhomogeneities in the strain distribution, and a high threading dislocation density. Our elastically strain-sharing Si(110) NMs, under optimal conditions, are likely to exhibit mobility improvements (7, 24) beyond what has been measured for similar strain levels because they have low surface/interface roughness, are virtually defect-free, and have uniform tensile strain; the hole mobility could reach well above 2.5 times the bulk Si(001) values for optimal structures (5). The introduction of local stressors in addition to the global strain created from elastic strain sharing would likely further improve charge carrier mobilities in (110)-oriented Si (9).

TABLE I. Structure of Si(110) NMs grown with MBE. The expected strain is calculated from Equation 1. The measured strain is extracted from the shift in the out-of-plane lattice constant.

Sample	Expected ε_{Si}	Measured ε_{Si}
9.5nm Si/49nm $Si_{.77}Ge_{.23}$/9.5 nm Si	0.63%	0.64 ± 0.09%
15nm Si/61nm $Si_{.83}Ge_{.17}$/14nm Si	0.43%	0.43 ± 0.08%
9nm Si/81nm $Si_{.88}Ge_{.12}$/10nm Si	0.33%	0.28 ± 0.05%
14nm Si/36nm $Si_{.79}Ge_{.21}$/12nm Si	0.45%	0.46 ± 0.03%

Conclusion

We have shown that we can controllably induce 'global' tensile strain in Si(110) without the use of crystalline defects. Moderate amounts of strain in Si(110) were achieved by using low-temperature MBE growth to obtain thicker, fully strained SiGe(110) layers used for strain-sharing between two layers of thin Si. Characterization of the trilayer Si(110) NMs with XRD and AFM reveals uniform strain sharing and smooth surfaces, neither of which is possible with strained-Si(110) fabrication on relaxed SiGe(110) substrates. The inherent challenges in the relaxation of SiGe(110) make elastic strain sharing an ideal way to obtain low-defect, uniformly strained Si(110), which may be used to measure mobility enhancement as a function of strain without mobility limiting defects. Overall, Si(110) NMs provide a unique way to create uniform biaxial strain on (110)-oriented Si, which is not possible with other methods.

Acknowledgments

This research was supported by DOE, Grant #DE-FG02-03ER46028. Facilities support by NSF, MRSEC program, is acknowledged. DMP acknowledges support from the National Defense Science and Engineering Graduate (NDSEG) fellowship program and the NSF Graduate Research Fellowship program. SOI(110) materials were provided by G.K. Celler, Soitec-USA, Inc.

References

1. V. Chan, K. Rim, M. Ieong, S. Yang, R. Malik, Y.W. Teh, M. Yang, and Q. Ouyang, *Proceedings of 2005 IEEE Integrated Circuit Conference*, pp. 667-74 (2005).
2. M. Chu, Y. Sun, U. Aghoram, and S.E. Thompson, *Annu. Rev. Mater. Res.*, **39**, 203-29 (2009).
3. O. Weber, T. Irisawa, T. Numata, M. Harada, N. Taoka, Y. Yamashita, T. Yamamoto, N. Sugiyama, M. Takenaka, and S. Takagi, *IEDM 2007*, pp. 719 – 22, (2007).
4. T. Sato, Y. Takeishi, and H. Hara, *Phys. Rev. B: Condens. Matter*, **4,** 1950-60 (1971).
5. M. Yang, V.W.C. Chan, K.K. Chan, L. Shi, D.M. Fried, J.H. Stathis, A.I. Chou, E. Gusev, J.A. Ott, L.E. Burns, M.V. Fischetti, and M. Ieong, *IEEE Trans. Electron Devices*, **53,** 965-78 (2006**)**.
6. T. Mizuno, N. Sugiyama, T. Tezuka, Y. Moriyama, S. Nakaharai, and S. Takagi, *IEEE Trans. Electron Devices*, **52,** 367-74 (2005).
7. W. Haensch, E. J. Nowak, R. H. Dennard, P. M. Solomon, A. Bryant, O. H. Dokumaci, A. Kumar, X. Wang, J. B. Johnson, and M. V. Fischetti, *IBM J. Res. Dev.*, **50**, 339-61 (2006).
8. H. Irie, K. Kita, K. Kyuno, and A. Toriwni, *IEDM 2004*, pp. 225-8 (2004).
9. T. Mizuno, T. Irisawa, N. Hirashita, Y. Moriyama, T. Numata, T. Tezuka, N. Sugiyama, and S. Takagi, *IEDM*, 1-4 (2006).
10. E. A. Fitzgerald, Y.-H. Xie, D. Monroe, P. J. Silverman, J. M. Kuo, A. R. Kortan, F. A. Thiel, and B. E. Weir, *J. Vac. Sci. Technol., B*, **10,** 1807-19 (1992).
11. T. Tezuka, N. Sugiyama, and S. Takagi, *Appl. Phys. Lett.*, **79,** 1798-1800 (2001).
12. R. Hull, J.C. Bean, L. Peticolas, and D. Bahnck, *Appl. Phys. Lett.*, **59**, 964-6 (1991).
13. M.L. Lee, D. A. Antoniadis, and E. A. Fitzgerald, *Thin Solid Films*, **508**, 136-9 (2006).
14. N. Sugiyama, Y. Moriyama, S. Nakahari, T. Tezuka, T. Mizuno, and S. Takagi, *Appl. Surf. Sci.*, **224**, 188-92 (2004).
15. A.C. Opotowsky, S.A. Scott, C.S. Ritz, D.E. Savage, G.K. Cellar and M.G. Lagally, *New J. Phys.*, **9**, 270 (2007).
16. A. Elfving, M. Zhao, G. V. Hansson, and W.-X. Ni, *Appl. Phys. Lett*., **89**, 181901-1 (2006).
17. Y. Moriyama, N. Hirashita, N. Sugiyama, and S. Takagi, *Thin Solid Films*, **517,** 285-8 (2008).
18. V. Destefanis, D. Rouchon, J. M. Hartmann, A. M. Papon, L. Baud, A. Crisci, and M. Mermoux, *J. Appl. Phys*, **106**, 043508 (2009).

19. M.M. Roberts, L.J. Klein, D.E. Savage, K.A. Slinker, M. Friesen, G. Celler, M.A. Eriksson, and M.G. Lagally, *Nat. Mater.*, **5**, 388-93 (2006).
20. D.M. Paskiewicz, S.A. Scott, D.E. Savage, and M.G. Lagally, *unpublished.*
21. L.B. Freund and S. Suresh, *Thin Film Materials*, Cambridge University Press, (2003**)**.
22. M.H. Huang, C. Boone, M. Roberts, D. E. Savage, M.G. Lagally, N.Shaji, H.Qin, R. Blick, J.A. Nairn, and F. Liu, Adv. Mater., **17**, 2860-4 (2005).
23. J.W. Matthews and A.E. Blakeslee, *J. Cryst. Growth*, **27,** 118-25 (1974).
24. D. Monroe, Y.H. Xie, E.A. Fitzgerald, P.J. Silverman, and G.P. Watson, *J. Vac. Sci. Technol., B*, **11,** 1731-7 (1993**)**.
25. D.C. Houghton, *J. Appl. Phys.*, **70,** 2136-51 (1991).
26. R. Hull, J.C. Bean, L.J. Peticolas, D. Bahnck, B.E. Weir, and L.C. Feldman, *Appl. Phys. Lett.*, **61,** 2802-4 (1992).
27. J.M. Hartmann, M. Burdin, G. Rolland, and T. Billon, *J. Cryst. Growth*, **294,** 288-95 (2006**)**.
28. J. Tersoff and F.K. LeGoues, *Phys. Rev. Lett.,* **72**, 3570-3 (1994).
29. K. Arimoto, J. Yamanaka, K. Nakagawa, K. Sawano, Y. Shiraki, N. Usami, and K. Nakajima, *J. Cryst. Growth*, **301-302**, 343-8 (2007**)**.
30. K. Arimoto, M. Watanabe, J. Yamanaka, K. Nakagawa, K. Sawano, Y. Shiraki, N. Usami, and K. Nakajima, *Thin Solid Films*, **517**, 235-8 (2008).
31. J. C. Bean, L. C. Feldman, A. T. Fiory, S. Nakahara, and I. K. Robinson, *J. Vac. Sci. Technol. A*, **2,** 436-40 (1984).
32. H.-C. Yuan, M.M. Kelly, D.E. Savage, M.G. Lagally, G.K. Celler, and Z. Ma, *IEEE Trans. Electron Devices*, **55,** 810-5 (2008**)**.
33. M. Fatemi, *J. Cryst. Growth*, **169,** 261-8 (1996**)**.
34. J. Hornstra and W.J. Bartels, *J. Cryst. Growth*, **44,** 513-7 (1978**)**.